Cloud properties from Atmospheric Infrared Sounder and evaluation with Cloud-Aerosol Lidar and Infrared Pathfinder Satellite Observations

C. J. Stubenrauch, S. Cros, N. Lamquin, R. Armante, A. Chédin, C. Crevoisier, N. A. Scott

Cloud properties from Atmospheric Infrared Sounder and evaluation with Cloud-Aerosol Lidar and Infrared Pathfinder Satellite Observations

C. J. Stubenrauch,[1] S. Cros,[1] N. Lamquin,[1] R. Armante,[1] A. Chédin,[1] C. Crevoisier,[1] and N. A. Scott[1]

Received 6 February 2008; revised 13 May 2008; accepted 9 July 2008; published 15 October 2008.

[1] The Atmospheric Infrared Sounder (AIRS) onboard the NASA Aqua satellite was primarily designed to provide atmospheric temperature and water vapor profiles, and the high spectral resolution of this instrument also allows the retrieval of cloud properties (especially cirrus). We present a retrieval of cloud pressure and effective emissivity, based on a weighted χ^2 method using channels around the 15-micron CO_2 absorption band. The cloud property retrieval is applied to all data, and tests based on the retrieved parameters determine cloud amount in a second step. Cloud-Aerosol Lidar and Infrared Pathfinder Satellite Observations (CALIPSO), launched as part of the A-Train in 2006, made it possible to evaluate the AIRS retrieved cloud height by comparing it to the height of maximum backscatter and of the ''apparent middle'' of the highest cloud layer determined by CALIPSO. The retrieved cloud height of about 66% (80%) of AIRS high (low) clouds lies within 1.5 km of the apparent middle of the CALIPSO cloud layers. Comparing cloud pressures shows an agreement in cloud height of 72% (59%) for high (low) clouds within 75 hPa. Keeping in mind that (1) low clouds are geometrically thinner (less than 1 km) than high clouds (in general between 1.5 and 3 km), (2) high clouds are also much more heterogeneous, and (3) CALIPSO only samples a small fraction of the AIRS footprint, the comparison is very encouraging. Zonal averages of high-, midlevel-, and low-cloud amount are compared to those of other data sets for January and July. Compared to our cloud retrieval, distributions of cloud pressure provided by AIRS L2 data reveal a strong bias toward lower pressures for low clouds.

Citation: Stubenrauch, C. J., S. Cros, N. Lamquin, R. Armante, A. Chédin, C. Crevoisier, and N. A. Scott (2008), Cloud properties from Atmospheric Infrared Sounder and evaluation with Cloud-Aerosol Lidar and Infrared Pathfinder Satellite Observations, *J. Geophys. Res.*, *113*, D00A10, doi:10.1029/2008JD009928.

1. Introduction

[2] Only satellite observations offer a continuous survey of the state of the atmosphere over the whole globe. Most current satellite instruments are radiometers, measuring reflected, scattered and emitted radiation from the Earth's surface, atmosphere and clouds. In general, to convert the measured radiances into cloud properties, clouds first have to be distinguished from clear sky situations and then their properties have to be determined using inverse radiative transfer models. CO_2 sensitive channels of infrared (IR) vertical sounders allow the determination of cloud height and cloud emissivity of a single cloud layer (the uppermost cloud layer in the case of multilayer cloud scenes). The TIROS-N Operational Vertical Sounders (TOVS) onboard the NOAA polar satellites provide data since 1979, the Atmospheric InfraRed Sounder (AIRS) onboard Aqua since 2002 and the IR Atmospheric Sounding Interferometer (IASI) onboard METOP since 2006. Cloud property retrievals using these data rely on the principle that radiances measured from near the center of a CO_2 absorption band are only sensitive to the upper atmosphere while radiances from the wings of the band (away from the band center) successively probe lower levels of the atmosphere. Compared to other passive remote sensing instruments, the high spectral resolution of IR vertical sounders provides especially reliable properties (height, temperature and effective emissivity) of cirrus (semitransparent ice clouds), with optical thickness as low as 0.1, day and night [e.g., *Wylie et al.*, 1994; *Ackerman et al.*, 1995; *Smith et al.*, 1998; *Stubenrauch et al.*, 1999a; *Wylie and Menzel*, 1999; *Chung et al.*, 2000; *Stubenrauch et al.*, 2006; *Kahn et al.*, 2007a, 2007b]. The A-Train mission [*Stephens et al.*, 2002], consisting of several passive and two active remote sensing instruments in constellation with the Aqua satellite, provides a unique possibility to explore the geometrical thickness and multilayer structure of clouds. One of these active remote sensing instruments is the Cloud-Aerosol Lidar with Orthogonal Polarization (CALIOP) of the Cloud-Aerosol Lidar and Infrared Pathfinder Satellite

[1]Laboratoire de Météorologie Dynamique, Ecole Polytechnique, IPSL, CNRS, Palaiseau, France.

0148-0227/08/2008JD009928

Observations (CALIPSO) mission [*Winker et al.*, 2007]. This instrument is even sensitive to cirrus with optical thickness smaller than 0.1.

[3] We present a cloud property retrieval algorithm for AIRS, which is based on a weighted χ^2 method [*Stubenrauch et al.*, 1999b], providing pressure and effective emissivity of a single cloud layer (of the uppermost cloud layer in the case of multilayer clouds). It is applied to all data, and in a second step, tests based on retrieved variables decide whether the AIRS footprint is cloudy or mostly clear. These tests have been established by comparing clear and cloudy scenes within the AIRS footprints, distinguished by the lidar CALIOP of the CALIPSO mission.

[4] Section 2 describes the AIRS cloud property retrieval algorithm, which makes use of retrieved atmospheric temperature and water vapor profiles of the AIRS L2 data [*Susskind et al.*, 2003] and of simulated atmospheric spectral transmissivity profiles of the Thermodynamic Initial Guess Retrieval (TIGR) data set [*Chédin et al.*, 1985; *Chevallier et al.*, 1998]. Special attention is given to the proximity recognition between the retrieved atmospheric profiles and the ones collected in the TIGR data set. Section 3 presents the analysis of 1 year of collocated AIRS-CALIPSO data. CALIPSO data are used to choose tests to determine the AIRS cloud amount and to evaluate the AIRS cloud height. In section 4 we first present a sensitivity analysis of the AIRS cloud property retrieval by investigating effects of channel choice, uncertainty in the choice of atmospheric profile, cloud detection and spatial resolution. Then zonal distributions of high-, midlevel- and low-cloud amounts as well as geographical maps of monthly mean cloud pressure are compared to those determined from CALIPSO L2, AIRS L2 and Moderate Resolution Imaging Spectroradiometer (MODIS) cloud products as well as from cloud climatologies of the International Satellite Cloud Climatology Project (ISCCP) and TOVS Path-B. Conclusions are drawn in section 5.

2. AIRS Cloud Property Retrieval

2.1. Data

[5] Launched in May 2002 onboard the Earth Observing System (EOS) platform Aqua, the AIRS instrument [*Aumann et al.*, 2003; *Chahine et al.*, 2006] provides very high spectral resolution measurements of Earth emitted radiation in three spectral bands (3.74–4.61 micron, 6.20–8.22 micron and 8.80–15.40 micron) using 2378 channels with a spectral resolution given by $\Delta\lambda/\lambda = 0.0008$. A subset of AIRS L1B data of 324 selected channels is being distributed by the National Oceanic and Atmospheric Administration-National Environmental Satellite Data and Information Service (NOAA-NESDIS) [*Goldberg et al.*, 2003] and archived at Laboratoire de Météorologie Dynamique (LMD) since January 2003. The polar orbiting Aqua satellite provides observations at 0130 and 1330 local time (LT). The spatial resolution of these measurements is 13.5 km at nadir. Nine AIRS measurements (3 × 3) correspond to one footprint of the Advanced Microwave Sounder Unit (AMSU). AIRS L2 standard products include temperature at 28 pressure levels from 0.1 hPa to the surface and water vapor mixing ratios in 14 pressure layers from 50 hPa to the surface [*Susskind et al.*, 2003, 2006]. These atmospheric profiles were retrieved from cloud-cleared AIRS radiances [*Chahine et al.*, 2006] within each AMSU footprint. Validations with radiosonde data from the NOAA-NESDIS operational meteorological database archive [*Divakarla et al.*, 2006] and with Atmospheric Radiation Measurement (ARM) data [*Tobin et al.*, 2006] have shown that the accuracy is close to 1 K in 1-km layers for temperature and better than 15% in 2-km layers for water vapor. For the cloud property retrieval we have collocated the AIRS L1B radiance measurements with the AIRS L2 standard products (version 5).

2.2. The χ^2_w Method for the Determination of p_{cld} and ε_{cld}

[6] The cloud property retrieval provides cloud pressure p_{cld} and effective cloud emissivity ε_{cld} by minimizing χ^2_w in equation (1). χ^2_w is computed by summation over N wavelengths λ_i of the CO_2 absorption band around 15 μm.

$$\chi^2_w(\boldsymbol{p}_k) = \sum_{i=1}^{N} \left(\boldsymbol{I}_{cld}(\boldsymbol{p}_k,\lambda_i) - \boldsymbol{I}_{clr}(\lambda_i)\right)\cdot \varepsilon_{cld}(\boldsymbol{p}_k) - \left(\boldsymbol{I}_m(\lambda_i) - \boldsymbol{I}_{clr}(\lambda_i)\right)]^2 * \boldsymbol{W}^2(\boldsymbol{p}_k,\lambda_i). \quad (1)$$

[7] The measured radiance I_m is obtained from the AIRS L1B data. We have chosen AIRS channels corresponding closely to the five channels used in the TIROS-N Operational Vertical Sounder (TOVS) Path-B cloud retrieval, at wavelengths of 14.190, 14.002, 13.928, 13.279 and 10.901 micron (AIRS channels 193, 226, 239, 355 and 787). The weighting functions of these channels are shown in Figure 1 as the derivatives of the transmission function with respect to pressure. Figure 1 also presents a clear sky spectrum along the CO_2 absorption band of the AIRS channels, simulated for a tropical atmosphere by the Automatized Atmospheric Absorption Atlas (4A) radiative transfer model [*Scott and Chédin*, 1981] (operational version available at http://www.noveltis.net/4AOP). The channels used in this study are indicated in Figure 1 by large circles.

[8] I_{clr} is the radiance which would be measured by AIRS in the case of clear sky, and I_{cld} is the radiance emitted by a homogenous opaque single cloud layer, calculated for 29 assumed cloud pressure levels p_k above surface (984 hPa to 106 hPa). The determination of I_{clr} and I_{cld} is described in section 2.3. The accuracy in p_{cld} is limited to the pressure level step of about 25 to 35 hPa.

[9] Empirical weights $W(p_k, \lambda_i)$ reflect the effect of the brightness temperature uncertainty on the cloudy and clear radiances at each cloud level within the air mass class closest to the observation (see below). They are determined as in equations (8) and (10) of *Stubenrauch et al.* [1999b]. Minimizing χ^2_w in equation (1) is equivalent to $d\chi^2_w/d\varepsilon_{cld} = 0$, from which one can extract ε_{cld} as

$$\varepsilon_{cld}(\boldsymbol{p}_k) = \frac{\sum_{i=1}^{N} [\boldsymbol{I}_m(\lambda_i) - \boldsymbol{I}_{clr}(\lambda_i)]\cdot[\boldsymbol{I}_{cld}(\boldsymbol{p}_k,\lambda_i) - \boldsymbol{I}_{clr}(\lambda_i)]\cdot \boldsymbol{W}^2(\boldsymbol{p}_k,\lambda_i)}{\sum_{i=1}^{N} [\boldsymbol{I}_{cld}(\boldsymbol{p}_k,\lambda_i) - \boldsymbol{I}_{clr}(\lambda_i)]^2 \cdot \boldsymbol{W}^2(\boldsymbol{p}_k,\lambda_i)}. \quad (2)$$

The χ^2_w method was developed to take into account (1) the weighting functions of the different channels, (2) the growing

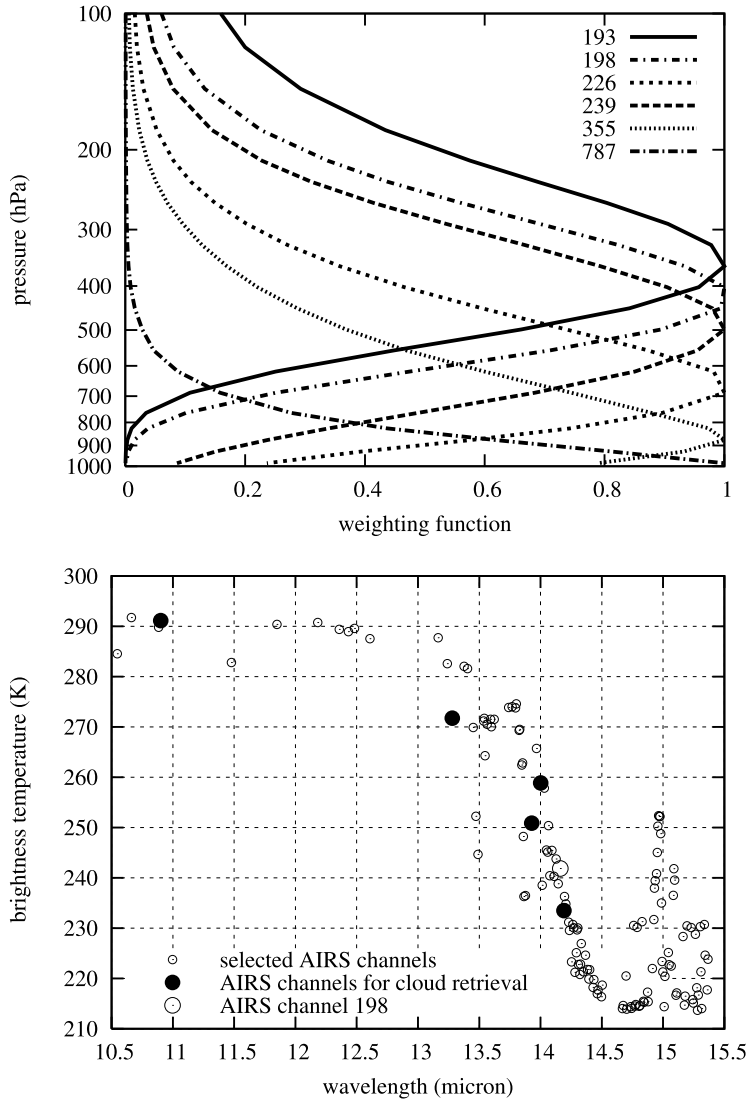

Figure 1. (top) Weighting functions of six AIRS channels, around the CO_2 absorption band at 15 μm, used in the cloud property retrieval. (bottom) Simulated clear sky brightness temperature spectrum; the six channels are indicated as big circles.

uncertainty in the computation of ε_{cld} with increasing p_k and (3) uncertainties in atmospheric profiles. When the χ^2_w method leads to a nonacceptable value of ε_{cld} (larger than 1.5), the scene is set to clear sky. It is important to allow values larger than 1, because at larger pressure levels I_{clr} and I_{cld} become very similar and their uncertainties can lead to values larger than 1 [see *Stubenrauch et al.*, 1999b].

2.3. Determination of I_{clr} and I_{cld}

[10] A crucial consideration in the cloud retrieval is the determination of I_{clr} and I_{cld}, since they depend strongly on the atmospheric condition. The AIRS-TIGR data set [*Chédin et al.*, 2003] archives atmospheric spectral transmissivity profiles at 40 pressure levels (from 1013 hPa to 0.05 hPa) at the 324 selected AIRS wavelengths, separately for each satellite viewing zenith angle. These values were simulated by the 4A radiative transfer model for about 2000 representative clear sky atmospheric temperature and humidity profiles out of about 200,000 operational meteorological radiosonde data collected by NOAA-NESDIS and the European Centre of Medium-range Weather Forecast (ECMWF). The 2000 atmospheric profiles were classified into five air masses (from tropical to polar). The use of these precomputed atmospheric spectral transmissivity profiles increases considerably the computation efficiency.

[11] The atmospheric spectral transmissivity profiles of the TIGR data set are used in combination with the AIRS L2 temperature profiles to determine I_{cld} at 29 pressure levels and I_{clr}. Therefore one has to determine the TIGR atmospheric profiles which are similar to the AIRS L2 atmospheric profiles.

[12] In the TOVS Improved Initialization Inversion (3I) algorithm [*Chédin et al.*, 1985; *Scott et al.*, 1999] a proximity recognition was performed by comparing the cloud-cleared observed brightness temperatures to the corresponding simulated clear sky brightness temperatures of the TIGR atmospheric profiles. At the time we developed the AIRS cloud property retrieval, the L2 cloud-cleared

radiances were not yet available. Therefore we developed a proximity recognition based on the comparison of the atmospheric temperature and water vapor profiles from AIRS L2 to those from TIGR, after interpolation of the AIRS L2 atmospheric profiles to the corresponding 4A pressure levels and layers. The TIGR atmospheric profile (out of P profiles of the corresponding air masses) which is declared as the most similar to the AIRS L2 atmospheric profile is the one for which the normalized distance *dist* in equation (3) is minimum.

$$\boldsymbol{dist}(\boldsymbol{n}) = \sqrt{\sum_{k=1}^{23} \frac{\left(\boldsymbol{T}_k^{TIGR}(\boldsymbol{n}) - \boldsymbol{T}_k^{AIRS}\right)^2}{\sigma(T_k)^2} + \boldsymbol{a}\sum_{l=1}^{8} \frac{\boldsymbol{b}_l\left(\boldsymbol{q}_l^{TIGR}(\boldsymbol{n}) - \boldsymbol{q}_l^{AIRS}\right)^2}{\sigma(\boldsymbol{q}_l)^2}}\, n = 1, P. \tag{3}$$

We use 23 levels k for temperature (T) from 1013 hPa to 70 hPa and eight layers l for water vapor (q) from 1013 hPa to 162 hPa. For higher surface elevations the number of levels and layers is reduced, beginning at the level closest but above surface. σ_{Tk} and σ_{ql} are the standard deviations of T_k and q_l of the TIGR profiles within the corresponding air mass. The sum of the water vapor differences has to be weighted by a owing to the difference in number of levels (23) and number of layers (8). Since water vapor in the upper troposphere is less important for the determination of radiances (or brightness temperatures, *TB*) than water vapor in the lower troposphere and since the uncertainty of AIRS L2 water vapor increases with height [*Gettelman et al.*, 2004], height-dependent weights b_l were introduced in equation (3).

[13] To determine the best values of constants a and b_l, we analyzed differences of mean brightness temperatures (or radiances) of clear sky, $TB_{clr}(\lambda_i)$, and opaque cloud at level k, $TB_{cld}(\lambda_i,p_k)$, between a reference atmospheric profile and the most similar atmospheric profiles according to equation (3). For this study we used the atmospheric profiles and atmospheric spectral transmissivity profiles of the AIRS-TIGR data set. Therefore we fixed one TIGR profile as reference profile (representative for the AIRS L2 atmospheric profile), applied equation (3) to determine the differences with each TIGR profile n, kept the TIGR profile with minimum *dist* ($dist_{min}$) and all TIGR profiles n with $dist(n) < 1.15\ dist_{min}$. Then the spectral transmissivity profiles of these atmospheric profiles similar to the reference profile were averaged, $(TB_{clr}(\lambda_i) - TB_{cld}(\lambda_i,p_k))_{\mathrm{prox}}$ computed and compared to $(TB_{clr}(\lambda_i) - TB_{cld}(\lambda_i,p_k))_{\mathrm{ref}}$ of the reference profile, for the five channels i used in the cloud property retrieval and for the 29 cloud pressure levels k. For a statistical analysis each TIGR atmospheric profile was used once as a reference profile. Figure 2 highlights the impact of the choice of a and b_l, by presenting averages of these *TB* differences at the 29 atmospheric cloud levels for two different weights a (a = 2 top and a = 3 bottom) and two sets of weights b_l (constant b_l l = 1 left and height-dependent weights b_l right). The best proximity was achieved by using $a = 2$ and $b_l = 1$ for $1 \le l \le 5$, $b_6 = 0.3$, $b_7 = 0.2$ and $b_8 = 0.1$, as can be seen in Figure 2 (top right).

[14] The clear and cloudy radiances in equations (1) and (2) are then determined by using the retrieved AIRS L2 temperature profile and the atmospheric transmissivities averaged over the TIGR profiles for which *dist* lies within 15% of the minimum difference $dist_{\min}$, using equation (3). We only use retrieved atmospheric AIRS L2 profiles of good quality in water vapor and surface temperature: retrieved atmospheric temperature is of good quality at all pressure levels, moisture is determined with good quality (L2 moisture quality flag less than 2 [see *Susskind et al.*, 2006; *Tobin et al.*, 2006]), and the error on the surface temperature is less than 3 K over water and less than 5 K over land. If the atmosphere is too cloudy, the retrieved atmospheric profile may be of bad quality. In this case we replace the profile by a monthly average of all AIRS L2 atmospheric profiles with good quality within an area of 1° latitude and 1° longitude.

2.4. Bias Adjustment Corrections

[15] To determine ε_{cld} in equation (2) in a coherent way, systematic biases between observed and simulated radiances (due to uncertainties in the radiative transfer model and in instrument calibration) have to be removed by applying bias corrections to the measured AIRS radiances. These bias adjustment corrections were determined from collocated AIRS L1B data and radiosonde data collected by the European Centre of Medium-range Weather Forecast (ECMWF). For clear sky scenes, detected by multispectral brightness temperature differences [*Crevoisier et al.*, 2004; *Pierangelo et al.*, 2005], the AIRS brightness temperatures are compared to those simulated by 4A using the atmospheric profiles of the radiosondes. The differences are defined as bias adjustment corrections. They were determined separately for ocean, for land excluding desert and for desert. Desert scene type is detected by using a climatology of spectral surface emissivity [*Péquignot et al.*, 2008] determined from AIRS measurements. Monthly mean values are given at a spatial resolution of 0.5° latitude × 0.5° longitude. A scene is identified as "desert" when the surface emissivity at 8.217 micron (AIRS channel 1263) smaller than 0.92. At present, these bias corrections have been computed only for the latitude band from 30°N to 30°S. Therefore the cloud property retrieval has so far only been applied to the AIRS measurements in the subtropics and the tropics.

2.5. Cloud Temperature and Cloud Types

[16] Cloud temperature T_{cld} is determined from p_{cld}, using the AIRS L2 temperature profile. Cloud types are distinguished according to p_{cld} and ε_{cld}. High clouds are defined by $p_{cld} < 440$ hPa, midlevel clouds by 440 hPa $< p_{cld} < 680$ hPa and low clouds by $p_{cld} > 680$ hPa. High clouds may be further distinguished into high opaque clouds ($\varepsilon_{cld} > 0.95$), cirrus ($0.95 > \varepsilon_{cld} > 0.50$) and thin cirrus ($\varepsilon_{cld} < 0.5$).

3. Analysis of Collocated AIRS-CALIPSO Cloud Properties

3.1. Collocation of AIRS and CALIPSO Data

[17] The lidar CALIOP [*Winker et al.*, 2007] of the CALIPSO mission provides backscatter profiles at 532 nm and at 1064 nm, at a vertical resolution of about 30 m to 60 m. The size of the lidar footprints is about 90 m × 90 m. Horizontal sampling is 333 m along the track and about 1000 km orthogonal to the track (distance between two

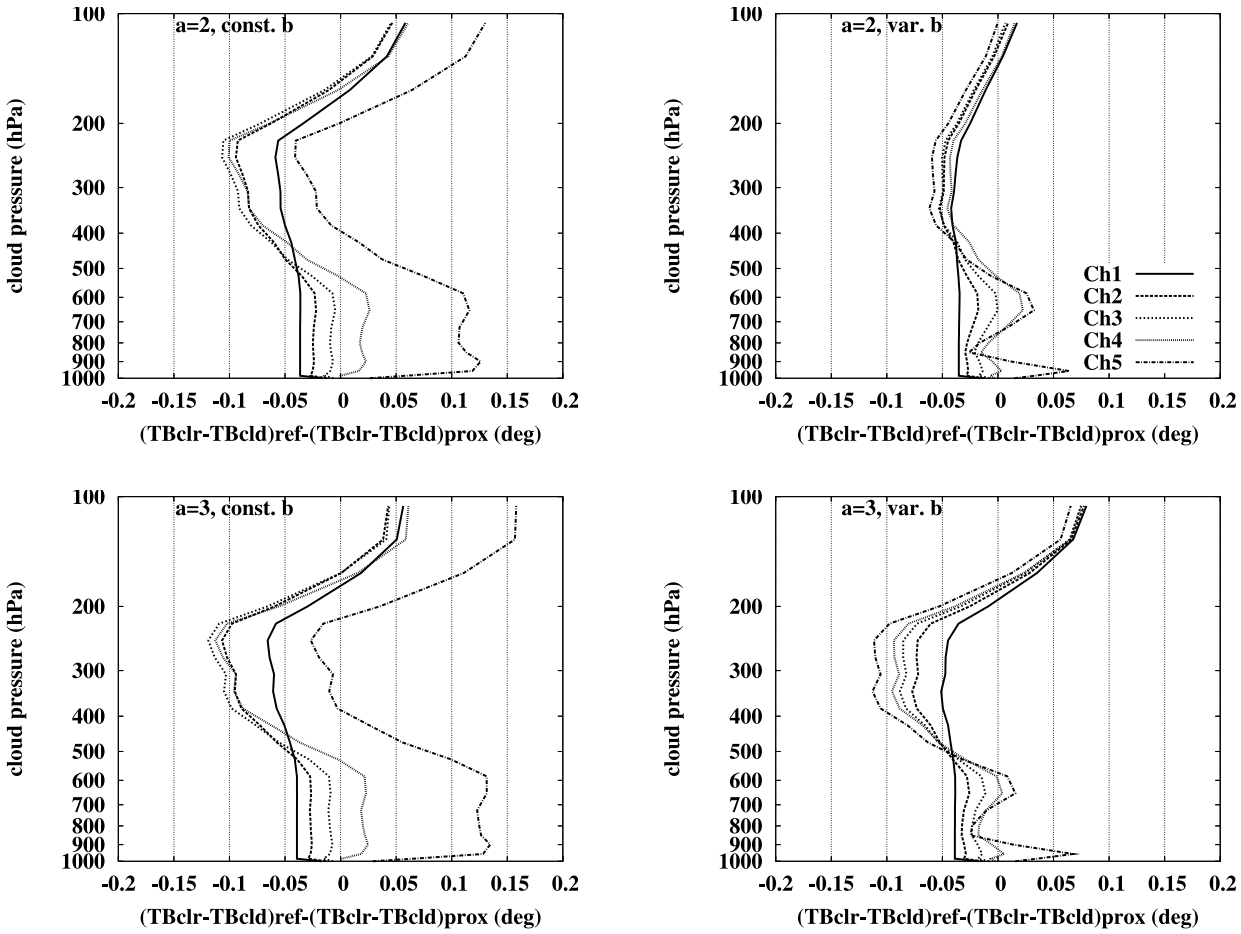

Figure 2. Mean differences of $(TB_{clr}(\lambda_i) - TB_{cld}(\lambda_i,p_k))_{\mathrm{ref}}$ and $(TB_{clr}(\lambda_i) - TB_{cld}(\lambda_i,p_k))_{\mathrm{prox}}$, for the five AIRS channels used in the cloud retrieval and for clouds assumed at 29 different pressure levels (on y axis). The impact of using different weights a and b_l in equation (3) for the proximity recognition are shown; (top) $a = 2$; (bottom) $a = 3$; (left) constant $b_l = 1$; and (right) variable b_l (1 for $1 \leq l \leq 5$, $b_6 = 0.3$, $b_7 = 0.2$, $b_8 = 0.1$).

orbits). The CALIPSO L2 cloud data (version 1) at 5 km resolution provide so far the number of cloud layers and the geometrical height of the cloud top, z_{top}, and of the "apparent" cloud base, z_{base}, of these layers, the latter corresponding to the cloud base or in the case of very thick clouds to the level to which the lidar penetrates downward. These values were transformed into cloud top pressure, p_{top}, and cloud base pressure, p_{base}, using the atmospheric profiles provided by the Global Modeling and Assimilation Office (GMAO), available in the CALIPSO L1 data. The pressure of the "apparent middle" of the cloud is then: $p_{mid} = 0.5(p_{top} + p_{base})$. The apparent middle could be slightly higher than the middle of the cloud in the case of very thick clouds, because the lidar signal does not completely penetrate the cloud. To distinguish between optically thin and thicker clouds, we have estimated the optical thickness τ_{vis} of the highest cloud layers. Therefore, first the apparent optical depth was computed from the difference between the signal below the highest cloud and the molecular signal at the same altitude. The molecular backscatter profiles were averaged over clear sky scenes within regions of 15° latitude × 15° longitude. In a second step, the apparent optical depth was corrected for multiple scattering contributions (by a factor of approximately 1.5 to 2.5 increasing with cloud optical depth). The uncertainty of the multiple scattering contribution is already about 20%. This is just a rough estimate of the optical thickness, but it can be used to distinguish between very thin clouds and thicker clouds. The procedure is described in detail by *Lamquin et al.* [2008]. Cloud optical thickness is provided by CALIPSO in version 2 of the data products. All satellites of the A-Train follow each other within a few minutes. In this constellation, the AIRS instrument is located in such a way that the AIRS footprints which are viewed under zenith angles between 13° and 20° are close to the CALIOP measurements, taken 75 s later than the ones by AIRS. For each of these AIRS footprints we choose the CALIPSO cloud product sample of 5 km resolution which is closest to the AIRS footprint center and which lies completely within its footprint. We have to keep in mind, however, that CALIPSO provides only a small sample (5 km × 90 m) of the AIRS footprint (14 km ×

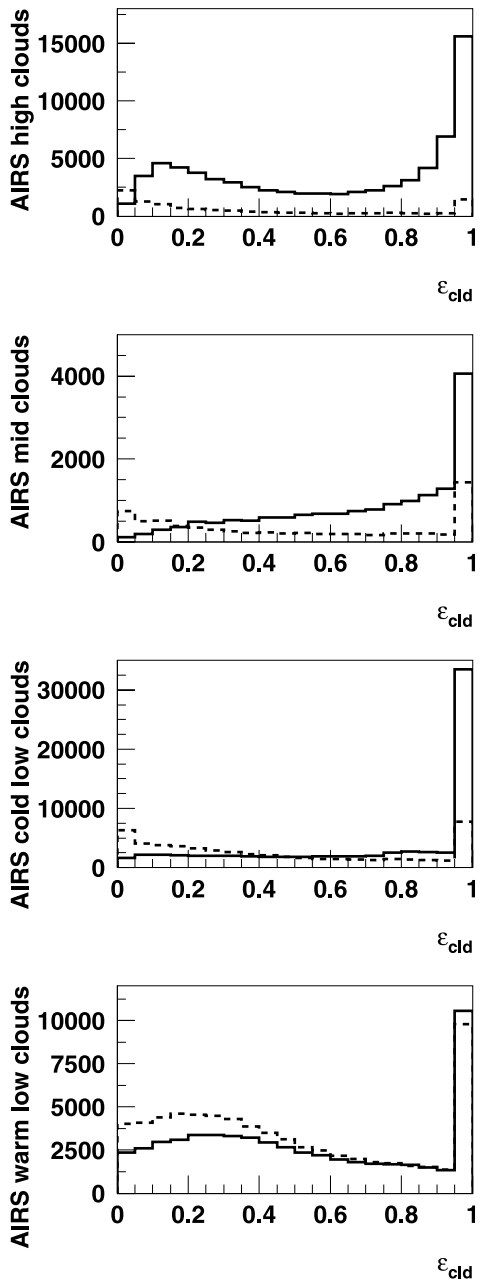

Figure 3. Distributions of ε_{cld} for AIRS high, midlevel, cold low, and warm low clouds for cases in which CALIPSO and AIRS agree ($|p_{cld} - p_{mid}| < 50$hPa) (solid line) and for cases which CALIPSO identifies as clear sky (no cloud layer found; dashed line). Cold and warm low clouds are distinguished by the threshold $T_{cld} - T_{surf}(air) = -4.5°C$.

14 km). Using a collocation of up to two CALIPSO samples within one AIRS footprint does not change the results (not shown), since the sample size is still very small. Since the performance of CALIOP is slightly better during night than during day [*Winker et al.*, 2007], we only analyze night data so far.

3.2. Determination of AIRS Cloud Amount

[18] Cloud detection based on multispectral brightness temperature differences was developed to discard cloudy scenes for CO_2 retrievals in the upper troposphere [*Crevoisier et al.*, 2004] and for aerosol retrievals in the lower troposphere [*Pierangelo et al.*, 2005]. Thresholds were chosen separately for ocean, for land excluding desert and for desert. Since this cloud detection was aimed at unambiguously identifying clear sky, it already identifies footprints as cloudy, which are covered by only a small fraction of cloud. Therefore it overestimates cloud amount, especially for low clouds (see Figure 9 in section 4.1).

[19] In the following we explore the possibility to design an "a posteriori" cloud detection which declares those footprints as cloudy for which one can determine the cloud properties in a reliable way (there should be more cloud than exposed surface in the footprint). Since the χ^2_w method can be applied to every AIRS footprint (without distinction of clear or cloudy), we use these results, in combination with the CALIPSO identification of clear sky and cloudy sky, to determine tests, mostly based on the retrieved variables, which distinguish between mostly cloudy AIRS footprints from those of clear sky or of situations for which it is difficult to determine cloud properties. The latter is the case when the IR contrast between cloud and surface is small, as in the case of partly cloudy low clouds and warm low clouds.

[20] First, all footprints for which the χ^2_w method yields a nonacceptable solution ($\varepsilon_{cld} > 1.5$; see section 2.2) are set to clear sky. This leads to a cloud amount of about 90% and to a relatively large low-cloud amount (see Figure 9 in section 4.1).

[21] In the following we explore variables for the distinction between mostly cloudy and mostly clear AIRS footprints. Figure 3 presents distributions of ε_{cld}, using 1 year of collocated AIRS-CALIPSO data, separately for AIRS high, midlevel and low clouds. Low clouds are further classified into cold and warm low clouds by considering $T_{cld} - T_{surf}(air)$. Cold low clouds are defined as clouds with $p_{cld} >$ 680 hPa and $T_{cld} - T_{surf}(air) < -4.5°C$. For each of these AIRS cloud types, distributions are shown for cases in which CALIPSO and AIRS agree ($|p_{cld} - p_{mid}| < 50$ hPa for the uppermost cloud of CALIPSO with $\tau_{VIS} > 0.1$; Figure 3, solid line) and for cases which CALIPSO identifies as clear sky (no cloud layers found in the sample of 5 km × 90 m; Figure 3, dashed line). When the AIRS footprint is identified as cloudy scene (high, midlevel or cold low clouds) by AIRS and as clear sky by CALIPSO, the distributions of ε_{cld} have a peak at 0. Distributions of scenes also identified as cloudy by CALIPSO have mostly larger values of ε_{cld}. However, one observes that for AIRS warm low clouds the distributions of ε_{cld} are similar for CALIPSO clear and cloudy scenes, and therefore ε_{cld} cannot be used anymore to distinguish between clear sky scenes and scenes of warm low clouds. One reason lies in the small contrast between cloud and surface in the IR. Figure 4 presents distributions of the difference between computed cloud emissivities at 12.183 micron and 10.901 micron (AIRS channels 528 and 787) for the same AIRS cloud types as in Figure 3, again for CALIPSO clear sky scenes and CALIPSO cloudy scenes. The cloud emissivities are computed as $\varepsilon_{cld}(\lambda) = [I_m(\lambda) - I_{clr}(\lambda)]/[I_{cld}(p_{cld}, \lambda) - I_{clr}(\lambda)]$. If the retrieved cloud pressure is correct, the difference should be small (and slightly positive) between the two wavelengths. Figure 4 shows again that for AIRS warm low clouds both

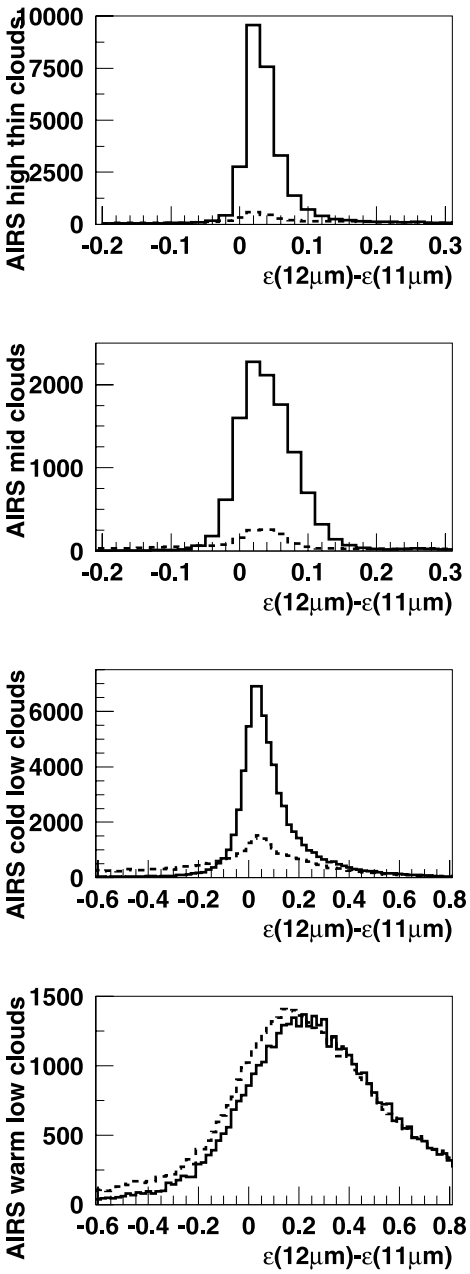

Figure 4. Distributions of computed cloud emissivity difference between 12 and 11 μm for AIRS high thin clouds ($\varepsilon_{cld} < 0.5$), AIRS midlevel, cold low, and warm low clouds, separately for cases in which CALIPSO and AIRS agree ($|p_{cld} - p_{mid}| < 50$hPa) (solid line) and for cases which CALIPSO identifies as clear sky (no cloud layer found; dashed line). Cold and warm low clouds are distinguished by the threshold $T_{cld} - T_{surf}(air) = -4.5°C$.

distributions (clear and for cloudy CALIPSO scenes) are very broad and similar, so that no distinction between clear sky and warm low clouds is possible. In addition we have explored a variable indicating the scene heterogeneity, computed from the mean brightness temperature at 10.901 micron and its standard deviation in the nine AIRS footprints per AMSU footprint: $0.01 \times MeanTB(10.901\ \mu m) \times \log(1 + \sigma(TB(10.901\ \mu m)))$, as in work by *Stubenrauch et al.* [1996]. This variable helps essentially to distinguish between clear scenes and midlevel cloud scenes (not shown). From these analyses we have defined the following tests, to be applied after the cloud retrieval and depending on the retrieved cloud type. If one of the following conditions is not fulfilled, the AIRS footprint is set to clear sky: for thin cirrus

$$\varepsilon_{cld} > 0.05$$
$$\varepsilon_{cld}(12.183\ \mu m) - \varepsilon_{cld}(10.901\ \mu m) > 0,$$

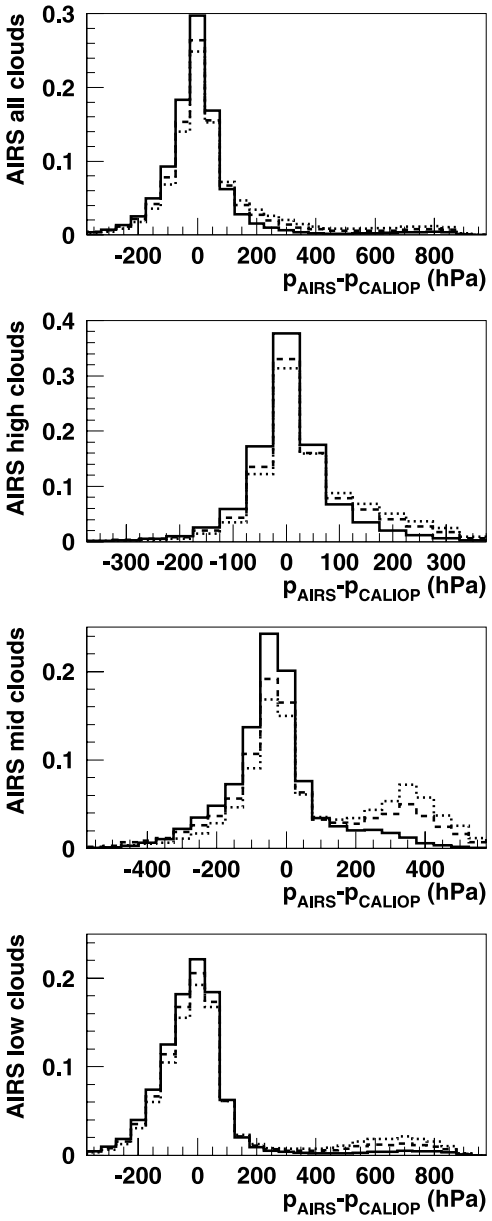

Figure 5. Normalized frequency distributions of the difference between AIRS p_{cld} and CALIPSO pressure of the middle of the cloud for all AIRS clouds, AIRS high, midlevel, and low clouds, compared to the highest cloud layer of all cloudy CALIPSO cases (dotted line), compared to the highest cloud layer with $\tau_{VIS} > 0.1$ (dashed line) and compared to the closest CALIPSO cloud layer (solid line). One year of collocated AIRS CALIPSO data within the latitude band 30°N–30°S are used.

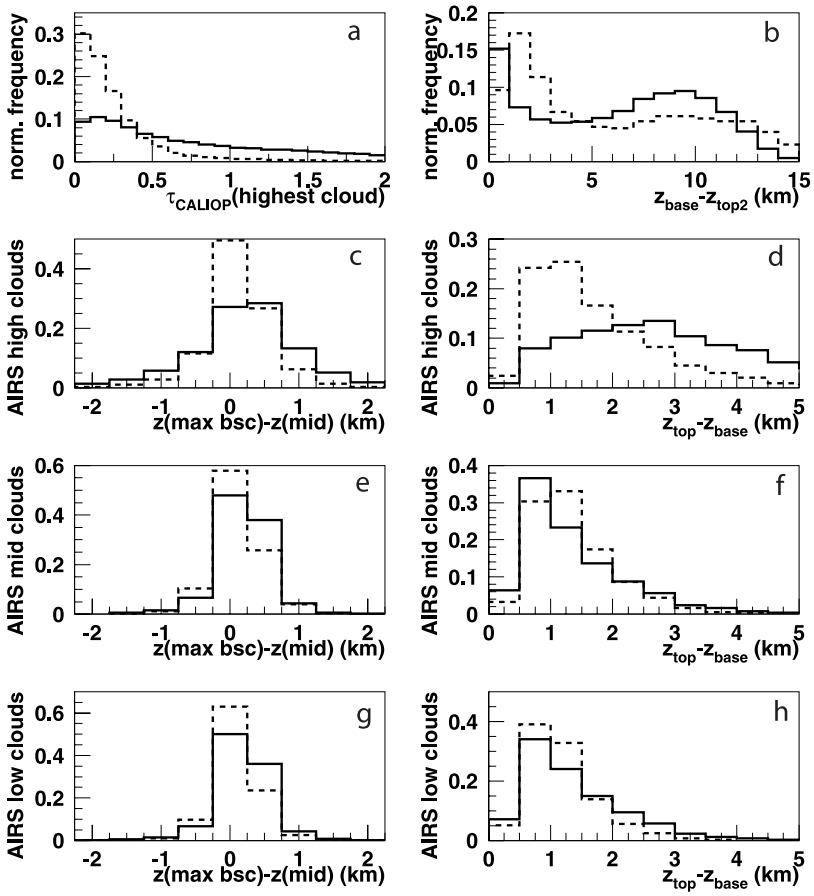

Figure 6. (a) Normalized frequency distributions of τ_{VIS} of the highest cloud layer, (b) height difference between base of the highest and top of the second highest layer, (c, e, g) difference between height of maximum backscatter and of the middle of the highest cloud layer for AIRS high, midlevel and low clouds and (d, f, h) geometrical cloud thickness of the highest cloud layer for AIRS high, midlevel, and low clouds for cases in which the closest CALIPSO cloud layer to the AIRS retrieved cloud height is the highest layer (solid line) and for cases in which the closest CALIPSO cloud layer to the AIRS retrieved cloud height is not the highest layer (dashed line).

for midlevel clouds

$$\varepsilon_{cld} > 0.10,$$
$$-0.02 < \varepsilon_{cld}(12.183\ \mu\mathrm{m}) - \varepsilon_{cld}(10.901\ \mu\mathrm{m}) < 0.15,$$
$$T_{cld} - T_{surf}(air) < -20^{\circ}\mathrm{C},$$
$$0.01 \times MeanTB(10.901\ \mu\mathrm{m}) \times \log(1 + \sigma(TB(10.901\ \mu\mathrm{m}))) > 3,$$

for low clouds

$$\varepsilon_{cld} > 0.10,$$
$$T_{cld} - T_{surf}(air) < -4.5^{\circ}\mathrm{C},$$
$$-0.6 < \varepsilon_{cld}(12.183\ \mu\mathrm{m}) - \varepsilon_{cld}(10.901\ \mu\mathrm{m}) < 0.6 \text{ over ocean},$$
$$-0.3 < \varepsilon_{cld}(12.183\ \mu\mathrm{m}) - \varepsilon_{cld}(10.901\ \mu\mathrm{m}) < 0.4 \text{ over land}.$$

3.3. Evaluation of AIRS Cloud Height

[22] An earlier comparison of cloud heights from the TOVS Path-B data set with quasi-simultaneous cloud heights of the uppermost cloud layers observed by the Lidar In Space Technology Experiment (LITE) onboard the space shuttle Discovery has revealed that (1) the cloud height determined by TOVS corresponds in general to the height of the apparent middle of the uppermost cloud of the scene and (2) clouds are detected as low as optical thickness τ_{VIS} of about 0.1 [*Stubenrauch et al.*, 2005].

[23] In this article we compare 1 year of collocated AIRS CALIPSO data. Figure 5 presents distributions of p_{cld}(AIRS) − p_{mid}(CALIPSO) for all AIRS clouds and separately for AIRS high, midlevel and low clouds. For each AIRS cloud type three distributions are shown: the AIRS cloud height is compared to (1) the highest cloud layer of all CALIPSO cloudy scenes (Figure 5, dotted line), (2) the highest cloud layer of CALIPSO clouds with $\tau_{VIS} > 0.1$ (Figure 5, dashed line) and (3) the CALIPSO cloud height which is closest to the AIRS cloud height, (only CALIPSO cloud layers with $\tau_{VIS} > 0.1$ are considered as in 2) (Figure 5, solid line). In general, the distributions peak around 0, and they get narrower from items 1 to 3. Especially cases with an uppermost high cloud identified by CALIPSO and a midlevel or low cloud by AIRS disappear, when the very thin clouds ($\tau_{VIS} \leq 0.1$) observed by CALIPSO are replaced by the clouds under-

Table 1. Frequency of Cases With AIRS Cloud Height and CALIPSO Cloud Height (of Maximum Backscatter Signal and of Apparent Middle of the Highest Cloud) Within 1.5 km[a]

	1		2		3	
	z(max bsc)	z(mid)	z(max bsc)	z(mid)	z(max bsc)	z(mid)
All clouds	56	58	61	62	68	70
Single layer	74	76	77	78		
Multilayer	28	30	37	39	56	57
$\varepsilon_{cld} > 0.6$	65	69	71	74	79	82
$\varepsilon_{cld} < 0.6$	44	43	47	45	54	52
AIRS high	46	51	50	55	61	66
Single layer	63	70	66	73		
Multilayer	32	34	37	40	58	60
$\varepsilon_{cld} > 0.6$	52	60	57	65	70	78
$\varepsilon_{cld} < 0.6$	41	42	43	44	52	53
AIRS mid	46	45	52	50	65	63
Single layer	70	67	72	69		
Multilayer	27	26	36	35	60	58
$\varepsilon_{cld} > 0.6$	58	59	66	67	84	84
$\varepsilon_{cld} < 0.6$	36	32	38	35	48	43
AIRS low	71	70	76	74	82	80
Single layer	83	81	85	83		
Multilayer	17	18	36	36	68	66
$\varepsilon_{cld} > 0.6$	80	81	85	85	91	91
$\varepsilon_{cld} < 0.6$	54	50	57	52	63	58

[a]Values given in percent. Cases: 1, highest cloud layer for all cloudy cases; 2, highest cloud layer with $\tau_{VIS} > 0.1$ and second highest in case of highest cloud layer with $\tau_{VIS} < 0.1$; and 3, cloud layer closest to AIRS. Values are shown for all AIRS clouds and AIRS high, midlevel, and low clouds. Distinction is also made between CALIPSO single cloud layer and multilayer cases and between AIRS thick clouds and thin clouds.

neath. When the closest layer is not the highest but the second highest layer, the highest layer is in general optically and geometrically thinner and often above another high cloud in the case of AIRS high clouds, as shown by the distributions in Figure 6. The comparison to the ''apparent middle height'' agrees slightly better for optically thick high clouds, whereas for optically thin low clouds the comparison to the height of maximum backscatter gives slightly better agreement (see Table 1). The difference is small, because both heights lie closely together, as shown in Figure 6. For high clouds however the height of maximum backscatter can be 1 km higher than the apparent middle of the cloud, especially for geometrically and optically thicker clouds. Two case studies [*Holz et al.*, 2006] using an improved CO_2 slicing cloud retrieval on measurements of the aircraft Scanning High-Resolution Interferometer Sounder (S-HIS) to determine the height of high clouds have shown that the retrieved cloud height corresponds to the level in the cloud where the Cloud Physics Lidar (CPL) integrated optical depth is approximately 1. This would mean that z_{cld}(AIRS) would be slightly smaller than z_{mid}(CALIPSO) for optically thick clouds and slightly larger than z_{mid}(CALIPSO) for optically thin clouds. Figure 7 presents distributions of z_{cld}(AIRS) − z_{mid}(CALIPSO), comparing the CALIPSO cloud layer which is closest to the AIRS cloud (only CALIPSO cloud layers with $\tau_{VIS} > 0.1$ are considered), separately for AIRS clouds with $\varepsilon_{cld} > 0.6$ (Figure 7, solid line) and for AIRS clouds with $\varepsilon_{cld} \leq 0.6$ (Figure 7, dashed line). The distributions peak around 0 for all AIRS clouds with $\varepsilon_{cld} > 0.6$ and also for AIRS high clouds with $\varepsilon_{cld} \leq 0.6$. For AIRS midlevel and low clouds with $\varepsilon_{cld} \leq 0.6$ the distributions peak around 1 km, meaning that in these cases the AIRS cloud height is on average 1 km higher than the apparent middle of the cloud. For thin clouds the distributions are larger, probably because the cloud property determination gets more uncertain. However, for thin high clouds the AIRS cloud height retrieved by the χ^2_w method has no bias. Since for optically thin and optically thick clouds the peak

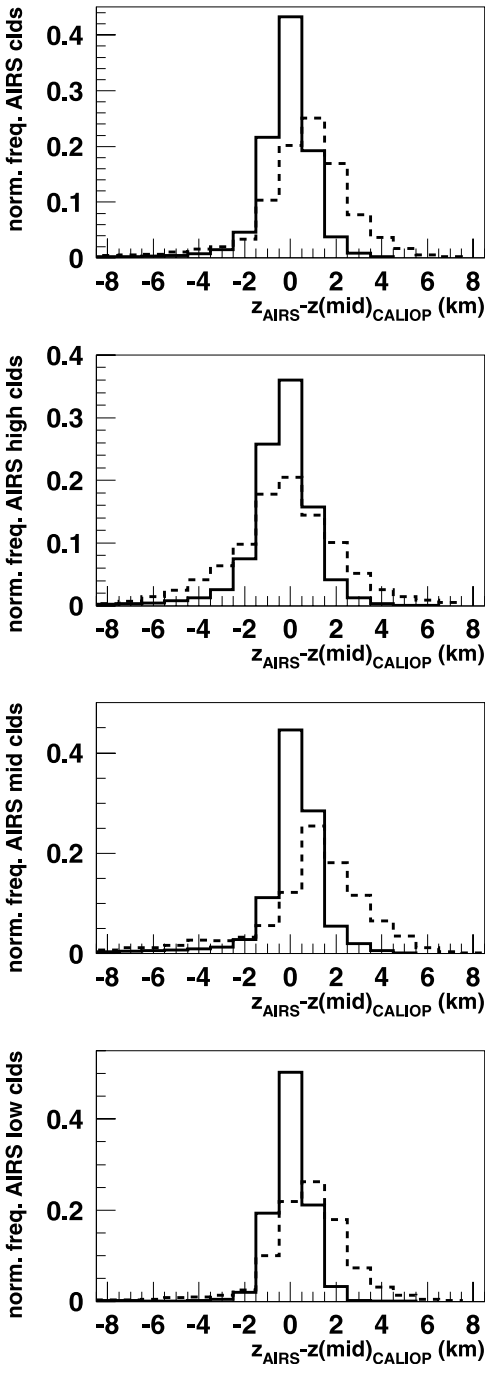

Figure 7. Normalized frequency distributions of the difference between AIRS z_{cld} and CALIPSO height of the apparent middle of the closest cloud layer with $\tau_{VIS} > 0.1$ for all AIRS clouds and for AIRS high, midlevel, and low clouds, separately for clouds with $\varepsilon_{cld} > 0.6$ (solid line) and clouds with $\varepsilon_{cld} < 0.6$ (dashed line).

Table 2. Frequency of Cases With AIRS Cloud Height and CALIPSO Cloud Height (of Apparent Middle of the Highest Cloud) Within 75 hPa[a]

	1	2	3
	p(mid)	p(mid)	p(mid)
All clouds	54	57	64
Single layer	65	67	
Multilayer	37	43	59
$\varepsilon_{cld} > 0.6$	62	67	73
$\varepsilon_{cld} < 0.6$	43	45	51
AIRS high	60	63	72
Single layer	76	79	
Multilayer	45	50	67
$\varepsilon_{cld} > 0.6$	65	70	81
$\varepsilon_{cld} < 0.6$	53	54	63
AIRS mid	38	43	53
Single layer	56	58	
Multilayer	24	31	49
$\varepsilon_{cld} > 0.6$	55	62	77
$\varepsilon_{cld} < 0.6$	24	25	32
AIRS low	51	54	59
Single layer	59	61	
Multilayer	16	28	50
$\varepsilon_{cld} > 0.6$	61	64	69
$\varepsilon_{cld} < 0.6$	33	34	38

[a]Values are given in percent. Cases: 1, highest cloud layer for all cloudy cases; 2, highest cloud layer with $\tau_{VIS} > 0.1$ and second highest in case of highest cloud layer with $\tau_{VIS} < 0.1$; and 3, cloud layer closest to AIRS. Values are shown for all AIRS clouds, AIRS high, midlevel, and low clouds. Distinction is also made between CALIPSO single cloud layer and multilayer cases and between AIRS thick clouds and thin clouds.

of the distribution is around 0, the difference between the height corresponding to the integrated optical depth of 1 and the apparent middle of the cloud seems to be within the bin width of 1 km.

[24] Table 1 shows the agreement of AIRS and CALIPSO cloud heights (of maximum backscatter and of apparent middle of the highest cloud) within 1.5 km, for the three comparison analyses as in Figures 5 and 7. The normalized frequencies of agreement within 1.5 km are shown separately for all AIRS clouds and then for AIRS high, midlevel and low clouds. Table 1 also distinguishes results for single layer and multilayer clouds (determined by CALIPSO) and for optically thick and thin clouds (determined by AIRS). The agreement within 1.5 km is better for low clouds (80%) than for high clouds (66%). The most important reason for this is that 1.5 km corresponds to about 50 hPa in the upper troposphere and to about 150 hPa in the lower troposphere. Comparing cloud pressures in Table 2 shows that the agreement within 75 hPa is slightly better for high clouds (72%) than for low clouds (59%). The agreement for high clouds is only slightly better than that for low clouds, because in general high clouds are also more heterogeneous and low clouds are geometrically thinner (less than 1 km) than high clouds (in general between 1.5 and 3 km). For $\varepsilon_{cld} > 0.6$ the agreement improves for high clouds to 78% (within 1.5 km) and 81% (within 75 hPa) and for low clouds to 91% (within 1.5 km) and 69% (within 75 hPa). The height determination of single layer high clouds (73% within 1.5 km and 79% within 75 hPa) is also better than for high clouds above other clouds (60% within 1.5 km and 67% within 75 hPa). It is interesting to note that in the case of multilayer clouds there is a big improvement between taking the highest layer with $\tau_{VIS} > 0.1$ or the closest cloud layer. This can probably be explained by several thin layers of high cloud above another high cloud. The occurrence of such cloud structures should be further investigated using combined A-Train data. Most of the AIRS low clouds are single layer clouds (83%) and most of the AIRS high clouds are multilayer cloud systems (59%), according to CALIPSO. Keeping in mind that CALIPSO only samples a small fraction of the AIRS footprint, the comparison is very encouraging.

4. Zonal Cloud Type Amounts and Cloud Pressure

[25] The application of the χ^2_w method allows the estimation of an uncertainty for each p_{cld} and ε_{cld}, by considering the solution of the second smallest $\chi^2_w(p_k)$. Figure 8 presents zonal averages of the absolute difference between the first and the second solution of p_{cld}, separately over ocean (Figure 8, circles) and over land (Figure 8, triangles) and for January 2007 (Figure 8, solid symbols) and for July 2007 (Figure 8, open symbols). On average, the uncertainty is slightly smaller over ocean (40 hPa) than over land (45 hPa). Especially over land, the uncertainty over specific regions like desert can be increased, as one can see in Figure 8 between 10°N and 20°N in summer. In this region the error on the surface temperature is also elevated.

4.1. Sensitivity Analysis of AIRS Cloud Property Retrieval

[26] In the following we investigate the effect of channel choice, uncertainty in atmospheric profiles, cloud detection and spatial resolution on the AIRS cloud property retrieval. Therefore we make the corresponding changes in the retrieval procedure and compare then AIRS high-cloud amount (HCA), midlevel-cloud amount (MCA) and low-

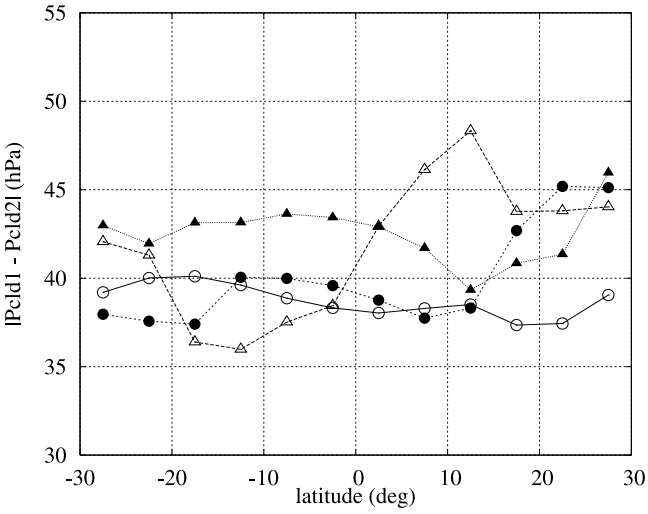

Figure 8. Zonal averages of absolute difference between p_{cld} of minimum χ_w^2 and p_{cld} of 2. Smallest $\chi_w^2(p_k)$, obtained from the LMD AIRS cloud retrieval, separately over ocean (circles) and over land (triangles) and for January 2007 (solid symbols) and for July 2007 (open symbols). This difference gives an estimate of the uncertainty of the retrieved p_{cld}.

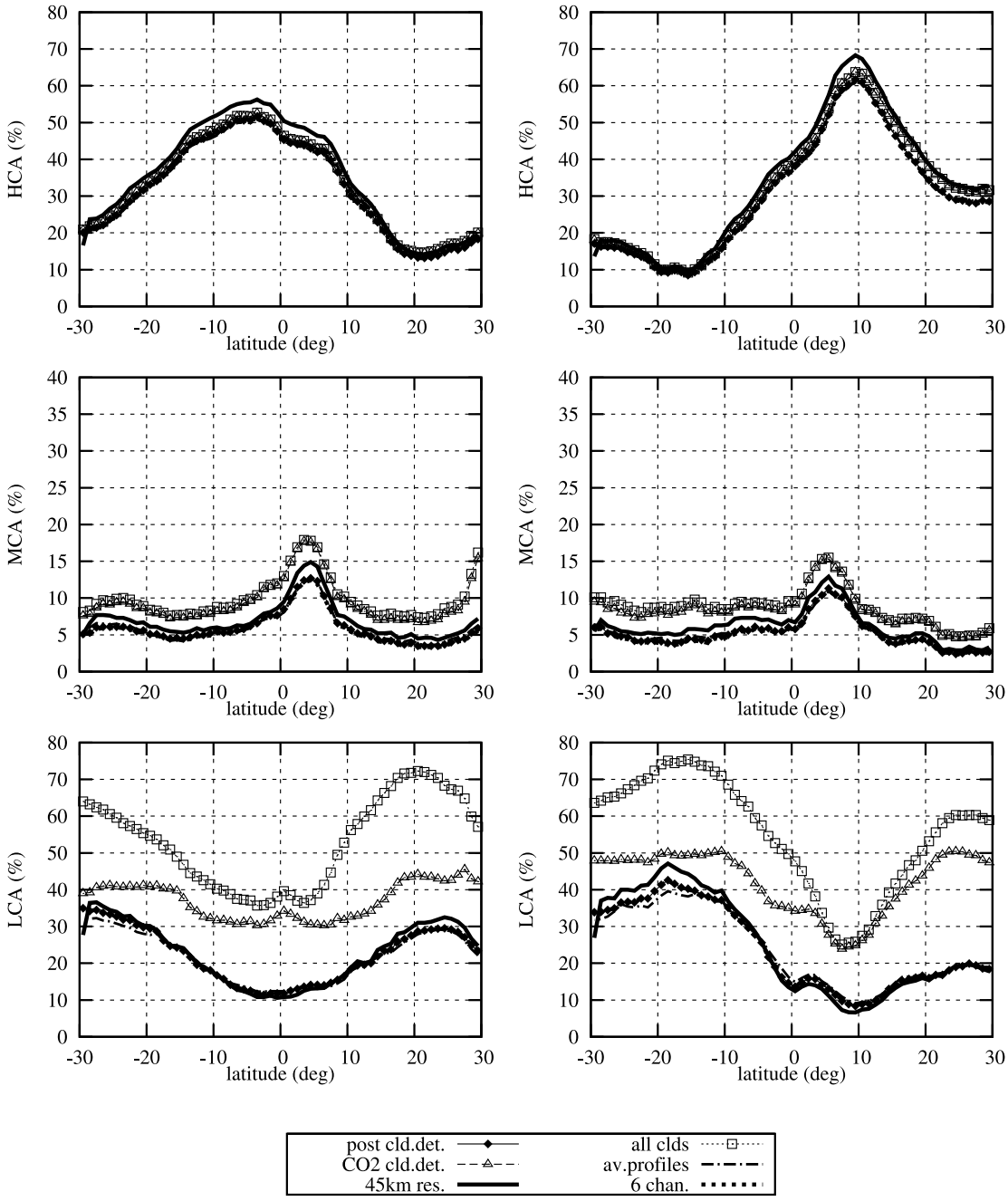

Figure 9. Zonal averages of high-cloud amount, midlevel-cloud amount, and low-cloud amount obtained from the AIRS LMD cloud retrieval, using six instead of five channels (6 chan.), using monthly average instead of instantaneous AIRS L2 atmospheric profiles (av. profiles), using a spatial resolution of 45 km instead of 13.5 km (45km res.), using all AIRS footprints providing a cw2 solution (all clds), using a multispectral cloud detection aimed at unambiguously identifying clear sky (CO2 cld. det.), and using the cloud detection described in section 3.2 (post cld. det.). (left) January 2007 and (right) July 2007.

cloud amount (LCA) as function of latitude in Figure 9 for (left) January 2007 and (right) July 2007.

[27] First we have examined the impact on the retrieved cloud properties when adding channels in the χ^2_w method. Figure 1 shows that AIRS channel 198 (corresponding to a wavelength of 14.162 micron) would slightly improve the vertical resolution in the middle to upper troposphere. However, cloud properties retrieved by using six (or even seven, not shown) channels are very similar to those using the initial five channels. The distribution of the p_{cld} difference is symmetrical with a peak around 0 hPa and a standard deviation of 11 hPa. A more detailed study involves the use of many more channels (see spectrum of Figure 1) in combination with an improvement of the vertical resolution of the TIGR data set. This is planned for the future.

[28] We have also investigated the effect of the choice of the coefficients a and b_l in equation (3) for the proximity

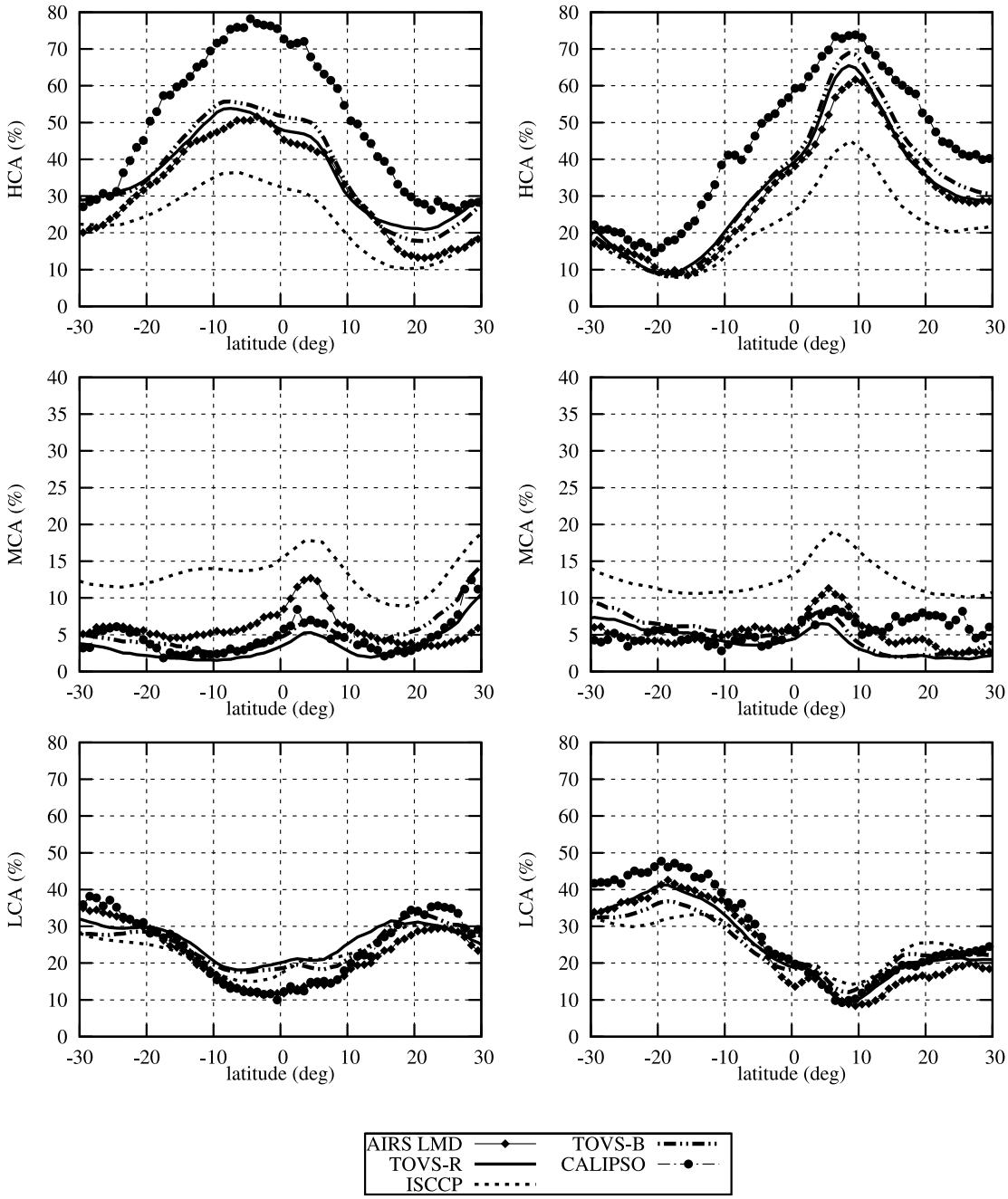

Figure 10. Zonal averages of high-cloud amount, midlevel-cloud amount, and low-cloud amount for (left) January and (right) July. Compared are results obtained from the AIRS LMD cloud retrieval (2007), CALIPSO L2 data (2007), TOVS Path-B and reanalyzed TOVS climatological values (1987–1995), and ISCCP climatological values (1987–1995).

recognition between the AIRS L2 and the TIGR atmospheric profiles. Therefore we have replaced first $a = 2$ (case described Figure 2, top right) by $a = 3$ (Figure 2, bottom right), and in a second analysis we have replaced the cloud height-dependent b_l (Figure 2, top left) by constant b_l (Figure 2, top right). In both cases the zonal averages of HCA, MCA and LCA are nearly identical (not shown). Another sensitivity concerning the uncertainty in atmospheric profiles has been studied by replacing the instantaneous AIRS L2 atmospheric profiles of good quality by monthly averages. As can be seen in Figure 9, the zonal averages of HCA, MCA and LCA are again not affected. The distribution of the p_{cld} difference is again symmetrical with a peak around 0 hPa and a standard deviation of 115 hPa.

[29] Figure 9 shows that LCA is up to 30 percentage points larger when the cloud detection identifies more clouds (CO_2 multispectral cloud detection compared to the a posteriori cloud detection described in section 3.2). The largest LCA is obtained when the cloud retrieval is applied to all AIRS footprints (up to 25 percentage points larger than LCA using the CO_2 cloud detection). The effect is

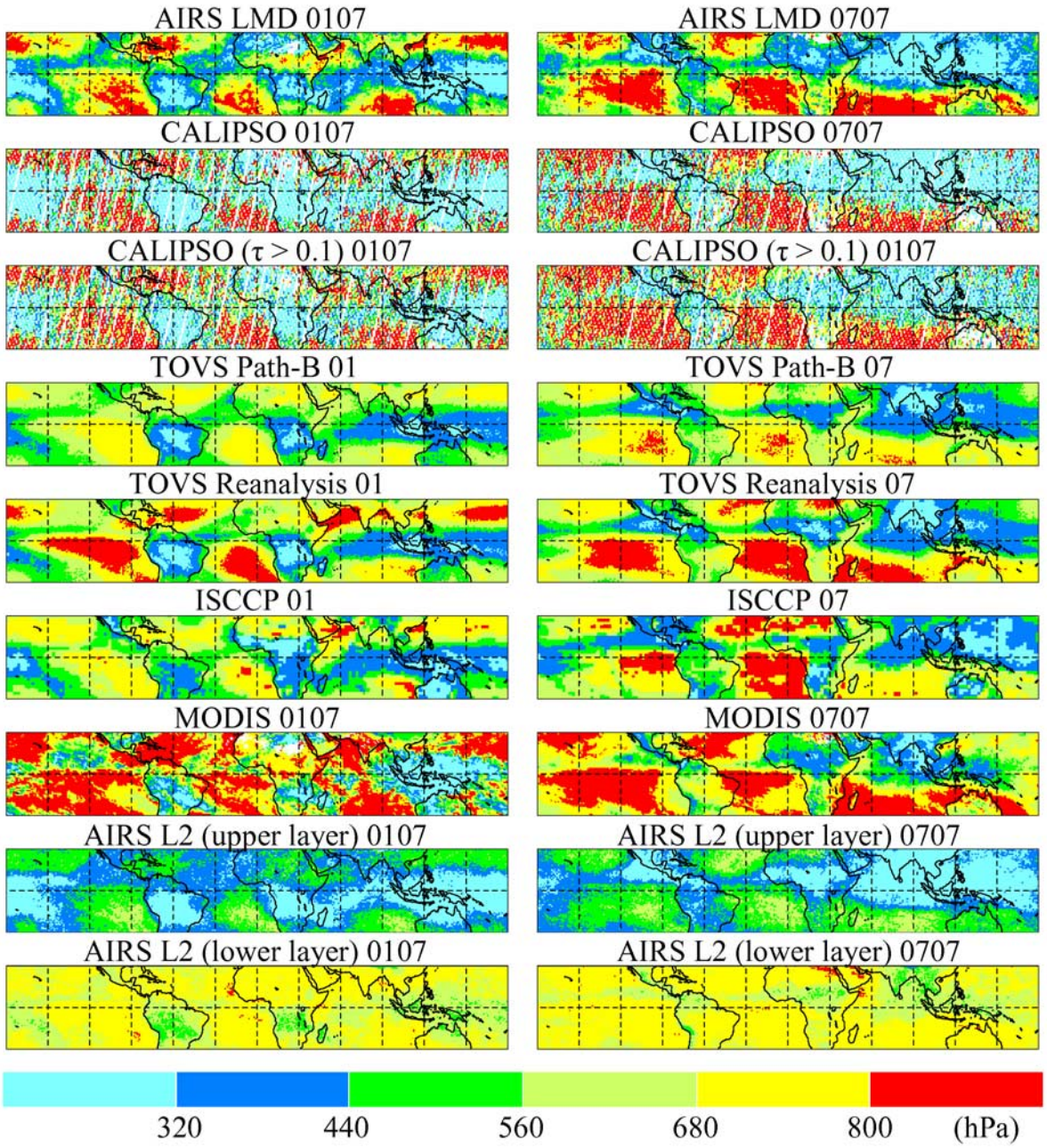

Figure 11. Geographical maps of monthly mean cloud pressure (in hPa) for (left) January and (right) July. Compared are results obtained from the AIRS LMD cloud retrieval (2007), from all CALIPSO L2 data and from CALIPSO L2 data with $\tau_{VIS} > 0.1$ (2007), from TOVS Path-B and reanalyzed TOVS climatological values (1987–1995), from ISCCP climatological daytime values (1987–1995), from MODIS (2007), and for the upper cloud levels and lower cloud levels of AIRS L2 data (2007).

much smaller on MCA (less than 5 percentage points) and negligible for HCA.

[30] Last we have investigated the effect of spatial resolution on the cloud property retrieval. For this study we have averaged the AIRS radiances over the nine AIRS footprints within each AMSU footprint. Then the cloud property retrieval and a posteriori cloud detection have been applied to the radiance averages. Thus we compare a spatial resolution at nadir of 13.5 km to one of about 45 km. It is interesting to note that the worsening of the spatial resolution leads to slightly more high clouds (identified as thin cirrus) in the region of the Intertropical Convergence Zone (ITCZ). The other cloud amounts are less affected.

4.2. Comparisons With Other Data Sets

[31] There exist several satellite climatologies providing cloud properties. ISCCP [*Rossow and Schiffer*, 1999] makes use of imagers on geostationary and polar orbiting weather satellites from 1983 to 2005. We determine climatological averages of monthly mean cloud pressure, HCA, MCA and LCA from cloud type statistics (during daytime) given in

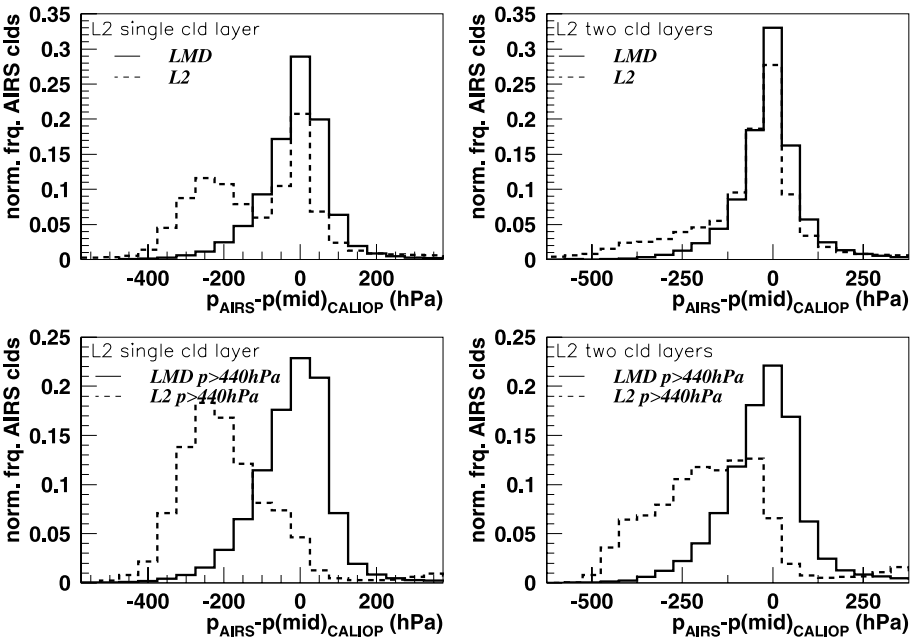

Figure 12. Normalized frequency distributions of the difference between AIRS-LMD p_{cld} and CALIPSO pressure of the apparent middle of the closest cloud layer with $\tau_{VIS} > 0.1$ and between AIRS-L2 p_{cld} and CALIPSO pressure of the apparent middle of the closest cloud layer with $\tau_{VIS} > 0.1$, separately for cases with (left) a single layer cloud and (right) multilayer clouds as determined by AIRS L2, (top) for all AIRS clouds and (bottom) for AIRS midlevel and low clouds. One year of collocated AIRS CALIPSO data within the latitude band 30°N–30°S are used.

the ISCCP D2 data over the period from 1987 to 1995 (as for TOVS Path-B; see next paragraph) for January and for July.

[32] The TOVS Path-B climatology [*Scott et al.*, 1999; *Stubenrauch et al.*, 2006] is established from TIROS-N Operational Vertical Sounder measurements onboard the polar orbiting NOAA satellites and covers at present the period from 1987 to 1995. The TOVS Path-B data set has been recently reanalyzed (TOVS-R), using improved radiative transfer model 4A, spectroscopy (the Geisa data bank) [*Jacquinet-Husson et al.*, 2003], TIGR data set and resulting bias correction constants. In fact, the same version of the 4A radiative transfer model, spectroscopy and TIGR data set have been used in the AIRS cloud retrieval at LMD. The TOVS-R results are also shown in the comparison, and they are similar to the ones of TOVS Path-B.

[33] Figure 10 presents HCA, MCA and LCA as function of latitude, separately for January (left) and for July (right) from the AIRS LMD retrieval, TOVS Path-B, TOVS-R, ISCCP and CALIPSO. HCA, MCA and LCA from CALIPSO are determined by using only the highest cloud layer. The results from AIRS and TOVS are very similar. ISCCP identifies slightly less high clouds and more midlevel clouds. This is due to scenes with thin cirrus above low clouds which are misidentified by ISCCP as midlevel clouds whereas IR sounders owing to their good spectral resolution determine the properties of the cirrus [*Stubenrauch et al.*, 1999a]. CALIPSO provides the largest HCA, because the active lidar instrument is more sensitive to thin cirrus than the IR sounders. LCA from all data sets agree within 10 percentage points.

[34] The MODIS instruments onboard the NASA Terra and Aqua satellites provide cloud properties [*King et al.*, 2003; *Platnick et al.*, 2003] since 2000. We use MYD08-M3 (from Aqua observed at 0130 LT) monthly averages of cloud pressure for January and July 2007.

[35] AIRS L2 data (version 5) provide in addition to the atmospheric profiles also effective cloud amount per AIRS footprint and cloud pressure [*Susskind et al.*, 2006] per AMSU footprint, for up to two different cloud layers.

[36] Figure 11 presents geographical maps of monthly mean p_{cld} for (left) January and (right) July, as provided by AIRS LMD, TOVS-R, TOVS Path-B, ISCCP and MODIS. For CALIPSO monthly mean p_{cld} is shown as average of the highest cloud layers and as average of the highest cloud layer with $\tau_{VIS} > 0.1$. For AIRS L2 monthly mean p_{cld} is shown as average of the upper layer and as average of the lower layer (in the case of two layers, in about 60 to 65% of all cloudy situations).

[37] Average p_{cld} gives an indication where the ITCZ with its high clouds is placed: over South America, Africa and Indonesia in January and north of the equator and over South Asia in July. These structures are more or less pronounced for the different data sets by low average p_{cld}. The sampling of CALIPSO is such that there is only about one data point per month (at 0130 LT). This explains the missing of p_{cld} values in the middle range, which are mostly obtained by averaging p_{cld} of high and low clouds over a month (especially if averaged over several years as in the climatologies). The geographical structures look quite similar to those of AIRS LMD, but the regions of high clouds are more extended. When replacing the highest cloud layer by the highest cloud layer with $\tau_{VIS} > 0.1$, the geographical pattern of mean p_{cld} is very similar, which shows that laminar cirrus which have already been observed by LITE

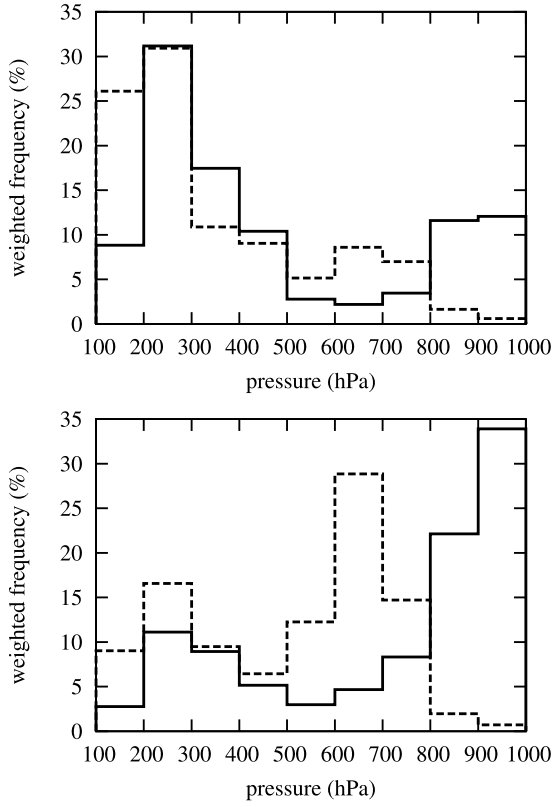

Figure 13. Frequency distributions of p_{cld} obtained from the AIRS LMD cloud retrieval (solid line), weighted by ε_{cld}, compared to those obtained from the highest cloud layers of the AIRS L2 data (dashed line), weighted by effective cloud amount, separately for the latitude bands (top) 0°–30°N and (bottom) 0°–30°S, in July 2007. AIRS LMD cloud properties are retrieved per AIRS footprint; L2 data provide p_{cld} for up to two cloud layers per AMSU footprint.

[*Winker and Trepte*, 1998] are often above thicker cirrus. Compared to MODIS, AIRS LMD seems to pick up much more high clouds, especially in July. The larger averages of p_{cld} from MODIS could also be explained by a cloud detection which detects more clouds, since the MODIS cloud amount is larger than the other cloud amounts (not shown). However, average p_{cld} of MODIS is smaller than average p_{cld} of the other data sets (except AIRS L2) in the Stratocumulus regions in the subtropics off the West coasts of South America and Africa. This has to be further investigated.

[38] The average p_{cld} of the upper AIRS L2 cloud layer (with effective cloud amount > 2%) shows more similarity in geographical structure to AIRS LMD than to MODIS, but the range in p_{cld} is much smaller, as can be seen by the occurrence of only four of the six colors in the maps. The average p_{cld} of the lower cloud layer of AIRS L2 never exceeds 800 hPa, whereas MODIS, AIRS LMD, CALIPSO and TOVS-R show wide regions in the subtropics with average p_{cld} > 800 hPa.

[39] To investigate the differences in p_{cld} between AIRS-LMD and AIRS-L2 in more detail, Figure 12 presents normalized frequency distributions of p_{cld}(AIRS-LMD) − p_{mid}(CALIPSO) and p_{cld}(AIRS-L2) − p_{mid}(CALIPSO), comparing to the closest CALIPSO cloud layer with τ_{VIS} > 0.1, separately for cases with (left) a single layer cloud and (right) multilayer clouds as determined by AIRS L2, (top) for all AIRS clouds and for AIRS midlevel and low clouds. To improve the reliability of AIRS L2 clouds, only AIRS L2 clouds are considered with an effective cloud amount > 2%. Whereas the AIRS LMD cloud height and the one of CALIPSO agree very well for all clouds, the distribution of the difference between AIRS L2 and CALIPSO cloud height has two distinct peaks in the case of single layer clouds: one around 0 hPa (in the case of high clouds) and one around −300 hPa (in the case of lower clouds). For multilayer clouds (about 60–65%), the second peak is much less pronounced, because most of the multilayer clouds are high clouds, but by considering clouds with p_{cld} > 440 hPa the bias of p_{cld}(AIRS-L2) appears again clearly. Such a bias for low clouds in the AIRS L2 data has also been demonstrated by *Kahn et al.* [2007b].

[40] The difference in AIRS L2 and AIRS LMD cloud properties can also be quantified by considering normalized frequency distributions of p_{cld}, weighted by effective cloud amount averaged over the upper layer within the AMSU footprint (L2) and by ε_{cld} (LMD). These are presented in Figure 13 for July 2007 in the latitude bands (top) 0°–30°N and (bottom) 0°–30°S. The AIRS LMD distributions show a large peak around 250 hPa in the latitude band of the ITCZ (0°–30°N) and more low clouds with large frequencies between 800 and 1000 hPa in the latitude band of the winter hemisphere. The peaks around 250 hPa are similar for the AIRS L2 data, but AIRS L2 data provide more high clouds above 200 hPa. However, the peak for low clouds of AIRS L2 data lies between 600 and 700 hPa, which is about 300 hPa lower than the peak for low clouds of AIRS LMD.

5. Conclusions

[41] First results of the AIRS LMD cloud retrieval, using a weighted χ^2 method on the radiances around the 15 μm CO_2 absorption combined with AIRS L2 atmospheric temperature profiles and precomputed spectral transmissivity profiles from the TIGR data set, have been presented for night observations in a latitude band between 30°N and 30°S. One year of collocated CALIPSO cloud data have been used to determine tests based on retrieved variables to obtain cloudy AIRS pixels for which the cloud property retrieval provides reliable information. It is concluded that the contrast between surface and cloud in the IR gets too low to distinguish cloudy and clear sky scenes when $T_{cld} - T_{surf(air)} > -4.5$°C. Cloud height of the AIRS LMD cloud retrieval has then been evaluated using the height of the maximum backscatter signal and of the apparent middle of the highest cloud layer determined by CALIPSO. The agreement is improved when clouds with $\tau_{VIS} < 0.1$ are removed from the comparison. This indicates that IR sounders are slightly less sensitive to very thin cirrus than active lidar. For about 55% (74%) of all AIRS high (low) clouds the retrieved cloud height is within 1.5 km of the highest cloud layer of CALIPSO. The agreement is improved to 66% (80%), when comparing to the CALIPSO cloud layer which is closest to the AIRS retrieved cloud height. This is justified, when considering that CALIPSO only samples a small part of the AIRS footprint. Comparing cloud pressures shows an agreement in cloud height of 72% (59%) for high (low) clouds

within 75 hPa. For high clouds the agreement is slightly better when comparing to the 'apparent middle' of the cloud instead of to the height of the maximum backscatter signal. This is because the maximum backscatter signal can be as much as 1 km above the apparent middle of the cloud, especially in the case of optically thick clouds. High clouds are also geometrically thicker and more heterogeneous than low clouds. The cloud height is determined with less uncertainty in the case of thicker clouds and of single layer clouds, however, the height differences between AIRS and CALIPSO always peak around 0, indicating no bias, with exception of a part of AIRS thin midlevel and low clouds which are probably falsely identified thicker low clouds. This could be at edges of thin high clouds over low-level clouds which exist in the tropics quite often [*Mace and Benson-Troth*, 2002] or linked to the atmospheric AIRS L2 profiles. This has to be explored further.

[42] A sensitivity study of the effect of cloud detection has shown larger average p_{cld} and LCA when more clouds are detected. Worsening the spatial resolution leads to about 5 percentage points larger HCA in the region of the ITCZ. Adding more AIRS channels in the cloud property retrieval did not affect the results. Zonal averages of HCA, MCA and LCA agree quite well with the ones of TOVS Path-B and CALIPSO, with CALIPSO more sensitive to thin cirrus. HCA of ISCCP is 15 percentage points smaller in the region of the ITCZ, which is linked to thin cirrus above low clouds which are identified as midlevel clouds by ISCCP.

[43] The larger averages of p_{cld} from MODIS can be partly explained by a cloud detection which detects more clouds. The largest cloud pressure values of AIRS L2 peak between 600 and 700 hPa, whereas the ones of the AIRS LMD retrieval peak between 800 and 1000 hPa, the latter in very good agreement with CALIPSO.

[44] The evaluation of the AIRS LMD cloud retrieval using CALIPSO data has shown that the retrieved cloud height is close to the one of the apparent middle of the uppermost cloud layer, for all cloud heights. We now intend to extend the retrieval to day measurements, to higher latitudes and to the whole AIRS data period from 2003 onward.

[45] **Acknowledgments.** This work has been supported by C.N.R.S. and by CNES. The AIRS version 5 data were obtained through the Goddard Earth Sciences Data and Information Services (http://daac.gsfc.nasa.gov/AIRS/data_access.shtml), and the CALIPSO data were obtained through the Atmospheric Sciences Data Center (ASDC) at NASA Langley Research Center by the ICARE Thematic Center created by CNES (http://www-icare.univ-lille1.fr/) and its interface ClimServ created for Institut Pierre Simon de Laplace (http://climserv.ipsl.polytechnique.fr/). ISCCP data are available at http://isccp.giss.nasa.gov/. MODIS monthly averages MYD08-M3 were acquired using the GES-DISC Interactive Online Analysis Infrastructure (Giovanni) as part of the NASA Goddard Earth Sciences Information Services Center (DISC) (http://disc.sci.gsfc.nasa.gov/techlab/giovanni/). The authors thank all the corresponding teams for assistance and public release of data products. The authors also thank Stephane Marchand for technical support with the CALIPSO code and Joel Susskind for a discussion about cloud amount, as well as three anonymous reviewers for the improvement of the manuscript.

References

Ackerman, S. A., W. L. Smith, A. D. Collard, X. L. Ma, H. E. Revercomb, and R. O. Knuteson (1995), Cirrus cloud properties derived from high-spectral resolution infrared spectrometry during FIRE II, Part II: Aircraft HIS results, *J. Atmos. Sci.*, *52*, 4246–4263, doi:10.1175/1520-0469(1995)052<4246:CCPDFH>2.0.CO;2.

Aumann, H. H., et al. (2003), AIRS/AMSU/HSB on the Aqua mission: Design, science objectives, data products, and processing systems, *IEEE Trans. Geosci. Remote Sens.*, *41*, 253–264, doi:10.1109/TGRS.2002.808356.

Chahine, M. T., et al. (2006), AIRS: Improving weather forecasting and providing new data on greenhouse gases, *Bull. Am. Meteorol. Soc.*, *87*, 911–926, doi:10.1175/BAMS-87-7-911.

Chédin, A., N. A. Scott, C. Wahiche, and P. Moulinier (1985), The improved initialization inversion method: A high resolution physical method for temperature retrievals from satellites of the TIROS-N series, *J. Clim. Appl. Meteorol.*, *24*, 128–143, doi:10.1175/1520-0450(1985)024<0128:TIIIMA>2.0.CO;2.

Chédin, A., S. Serrar, N. A. Scott, C. Crevoisier, and R. Armante (2003), First global measurement of midtropospheric CO_2 from NOAA polar satellites: Tropical zone, *J. Geophys. Res.*, *108*(D18), 4581, doi:10.1029/2003JD003439.

Chevallier, F., F. Cheruy, N. A. Scott, and A. Chédin (1998), A neural network approach for a fast and accurate computation of longwave radiative budget, *J. Appl. Meteorol.*, *37*, 1385–1397, doi:10.1175/1520-0450(1998)037<1385:ANNAFA>2.0.CO;2.

Chung, S. G., S. A. Ackerman, P. F. Van Delst, and W. P. Menzel (2000), Model calculations and interferometer measurements of ice-cloud characteristics, *J. Appl. Meteorol.*, *39*, 634–644.

Crevoisier, C., S. Heilliette, A. Chédin, S. Serrar, R. Armante, and N. A. Scott (2004), Midtropospheric CO_2 concentration retrieval from AIRS observations in the tropics, *Geophys. Res. Lett.*, *31*, L17106, doi:10.1029/2004GL020141.

Divakarla, M. G., C. D. Barnet, M. D. Goldberg, L. M. McMillin, E. Maddy, W. Wolf, L. Zhou, and X. Liu (2006), Validation of Atmospheric Infrared Sounder temperature and water vapor retrievals with matched radiosonde measurements and forecasts, *J. Geophys. Res.*, *111*, D09S15, doi:10.1029/2005JD006116.

Gettelman, A., et al. (2004), Validation of Aqua satellite data in the upper troposphere and lower stratosphere with in situ aircraft instruments, *Geophys. Res. Lett.*, *31*, L22107, doi:10.1029/2004GL020730.

Goldberg, M. D., Y. Qu, L. M. McMillin, W. Wolf, L. Zhou, and M. Divakarla (2003), AIRS near-real-time products and algorithms in support of numerical weather prediction, *IEEE Trans. Geosci. Remote Sens.*, *41*, 379–389, doi:10.1109/TGRS.2002.808307.

Holz, R. E., S. Ackerman, P. Antonelli, F. Nagle, R. O. Knuteson, M. McGill, D. L. Hlavka, and W. D. Hart (2006), An improvement to the high-spectral-resolution CO_2-slicing cloud-top altitude retrieval, *J. Atmos. Oceanic Technol.*, *23*, 653–670, doi:10.1175/JTECH1877.1.

Jacquinet-Husson, N., N. A. Scott, A. Chédin, and A. A. Chursin (2003), The GEISA spectroscopic database system revisited for IASI direct radiative transfer modelling, *Atmos. Oceanic Opt.*, *16*, 256–282.

Kahn, B. H., A. Eldering, A. J. Braverman, E. J. Fetzer, J. H. Jiang, E. Fishbein, and D. L. Wu (2007a), Toward the characterization of upper tropospheric clouds using Atmospheric Infrared Sounder and Microwave Limb Sounder observations, *J. Geophys. Res.*, *112*, D05202, doi:10.1029/2006JD007336.

Kahn, B. H., et al. (2007b), Cloud type comparisons of AIRS, CloudSat and CALIPSO cloud height and amount, *Atmos. Chem. Phys. Discuss.*, *7*, 13,915–13,958.

King, M. D., et al. (2003), Cloud and aerosol properties, precipitable water, and profiles of temperature and water vapour from MODIS, *IEEE Trans. Geosci. Remote Sens.*, *41*, 442–458, doi:10.1109/TGRS.2002.808226.

Lamquin, N., C. J. Stubenrauch, and J. Pelon (2008), Upper tropospheric humidity and cirrus thickness: A statistical analysis using 1 year of collocated Atmospheric Infrared Sounder and Cloud-Aerosol Lidar and Infrared Pathfinder Satellite Observations data, *J. Geophys. Res.*, *113*, D00A08, doi:10.1029/2008JD010012.

Mace, G. G., and S. Benson-Troth (2002), Cloud overlap characteristics derived from long-term cloud radar data, *J. Clim.*, *15*, 2505–2515, doi:10.1175/1520-0442(2002)015<2505:CLOCDF>2.0.CO;2.

Péquignot, E., A. Chédin, and N. A. Scott (2008), Infrared continental surface emissivity spectra retrieved from AIRS hyperspectral sensor, *J. Appl. Meteorol. Climatol.*, *47*, 1619–1633.

Pierangelo, C., M. Mishchenko, Y. Balkanski, and A. Chédin (2005), Retrieving the effective radius of Saharan dust coarse mode from AIRS, *Geophys. Res. Lett.*, *32*, L20813, doi:10.1029/2005GL023425.

Platnick, S., M. D. King, S. A. Ackerman, W. P. Menzel, B. A. Baum, J. C. Riedi, and R. A. Frey (2003), The MODIS cloud products: Algorithms and examples from Terra, *IEEE Trans. Geosci. Remote Sens.*, *41*, 459–473, doi:10.1109/TGRS.2002.808301.

Rossow, W. B., and R. A. Schiffer (1999), Advances in understanding clouds from ISCCP, *Bull. Am. Meteorol. Soc.*, *80*, 2261–2287, doi:10.1175/1520-0477(1999)080<2261:AIUCFI>2.0.CO;2.

Scott, N. A., and A. Chédin (1981), A fast line-by-line method for atmospheric absorption computations: The 4A Automized Atmospheric Absorption Atlas, *J. Appl. Meteorol.*, *20*, 801–812.

Scott, N. A., A. Chédin, R. Armante, J. Francis, C. J. Stubenrauch, J.-P. Chaboureau, F. Chevallier, C. Claud, and F. Chéruy (1999), Characteristics of the TOVS Pathfinder Path-B Data set, *Bull. Am. Meteorol. Soc.*, *80*, 2679–2701, doi:10.1175/1520-0477(1999)080<2679:COTTPP>2.0.CO;2.

Smith, W. L., S. A. Ackerman, H. Revercomb, H. Huang, D. H. DeSlover, W. Feltz, L. Gumley, and A. D. Collard (1998), Infrared spectral absorption of nearly invisible cirrus clouds, *Geophys. Res. Lett.*, *25*, 1137–1140, doi:10.1029/97GL03491.

Stephens, G., et al. (2002), The CloudSat mission and the A-train, *Bull. Am. Meteorol. Soc.*, *83*, 1771–1790, doi:10.1175/BAMS-83-12-1771.

Stubenrauch, C. J., G. Sèze, N. A. Scott, A. Chédin, M. Desbois, and R. S. Kandel (1996), Cloud field identification for Earth radiation budget studies: II. Cloud field classification for the ScaRaB radiometer, *J. Appl. Meteorol.*, *35*, 428–443, doi:10.1175/1520-0450(1996)035<0428:CFIFER>2.0.CO;2.

Stubenrauch, C. J., W. B. Rossow, N. A. Scott, and A. Chédin (1999a), Clouds as seen by infrared sounders (3I) and imagers (ISCCP): Part III. Spatial heterogeneity and radiative effects, *J. Clim.*, *12*, 3419–3442, doi:10.1175/1520-0442(1999)012<3419:CASBSS>2.0.CO;2.

Stubenrauch, C. J., A. Chédin, R. Armante, and N. A. Scott (1999b), Clouds as seen by infrared sounders (3I) and imagers (ISCCP): Part II. A new approach for cloud parameter determination in the 3I algorithms, *J. Clim.*, *12*, 2214–2223, doi:10.1175/1520-0442(1999)012<2214:CASBSS>2.0.CO;2.

Stubenrauch, C. J., F. Eddounia, and L. Sauvage (2005), Cloud heights from TOVS Path-B: Evaluation using LITE observations and distributions of highest cloud layers, *J. Geophys. Res.*, *110*, D19203, doi:10.1029/2004JD005447.

Stubenrauch, C. J., A. Chédin, G. Rädel, N. A. Scott, and S. Serrar (2006), Cloud properties and their seasonal and diurnal variability from TOVS Path-B, *J. Clim.*, *19*, 5531–5553, doi:10.1175/JCLI3929.1.

Susskind, J., C. Barnet, and J. Blaisdell (2003), Retrieval of atmospheric and surface parameters from AIRS/AMSU/HSB data in the presence of clouds, *IEEE Trans. Geosci. Remote Sens.*, *41*, 390–409, doi:10.1109/TGRS.2002.808236.

Susskind, J., C. Barnet, J. Blaisdell, L. Iredell, F. Keita, L. Kouvaris, G. Molnar, and M. Chahine (2006), Accuracy of geophysical parameters derived from AIRS/AMSU as a function of fractional cloud cover, *J. Geophys. Res.*, *111*, D09S17, doi:10.1029/2005JD006272.

Tobin, D. C., H. E. Revercomb, R. O. Knuteson, B. M. Lesht, L. L. Strow, S. E. Hannon, W. F. Feltz, L. A. Moy, E. J. Fetzer, and T. S. Cress (2006), Atmospheric Radiation Measurement site atmospheric state best estimates for Atmospheric Infrared Sounder temperature and water vapor retrieval validation, *J. Geophys. Res.*, D09S14, doi:10.1029/2005JD006103.

Winker, D. M., and C. R. Trepte (1998), Laminar cirrus observed near the tropical tropopause by LITE, *Geophys. Res. Lett.*, *25*, 3351–3354, doi:10.1029/98GL01292.

Winker, D. M., W. H. Hunt, and M. J. McGill (2007), Initial performance assessment of CALIOP, *Geophys. Res. Lett.*, *34*, L19803, doi:10.1029/2007GL030135.

Wylie, D. P., and W. P. Menzel (1999), Eight years of cloud statistics using HIRS, *J. Clim.*, *12*, 170–184.

Wylie, D. P., W. P. Menzel, and K. I. Strabala (1994), Four years of global cirrus cloud statistics using HIRS, *J. Clim.*, *7*, 1972–1986, doi:10.1175/1520-0442(1994)007<1972:FYOGCC>2.0.CO;2.

R. Armante, A. Chédin, C. Crevoisier, S. Cros, N. Lamquin, N. A. Scott, and C. J. Stubenrauch, Laboratoire de Météorologie Dynamique, Ecole Polytechnique, IPSL, CNRS, F-91128 Palaiseau CEDEX, France. (stubenrauch@lmd.polytechnique.fr)